
Article:
Blitz, MA orcid.org/0000-0001-6710-4021, Salter, RJ, Heard, DE orcid.org/0000-0002-0357-6238 et al. (1 more author) (2017) An Experimental Study of the Kinetics of OH/OD(v=1,2,3) + SO_2: the Limiting High Pressure Rate Coefficients as a Function of Temperature. Journal of Physical Chemistry A, 121 (17). pp. 3175-3183. ISSN 1089-5639

https://doi.org/10.1021/acs.jpca.7b01294

An Experimental Study of the Kinetics of OH/OD(v=1,2,3) + SO_2: the Limiting High Pressure Rate Coefficients as a Function of Temperature

Mark A. Blitz,[a,b]* Robert J. Salter,[a,c] Dwayne E. Heard [a,b] and Paul W. Seakins [a,b]

[a] School of Chemistry, University of Leeds, Leeds, LS2 9JT, UK

[b] National Centre for Atmospheric Science, University of Leeds, Leeds, LS2 9JT, UK

[c] Now at Deloitee MCS, 3 Rivergate, Temple Quay, Bristol, BR1 6GD, UK

*E-mail: m.blitz@leeds.ac.uk

Abstract

The kinetics of the reaction OH/OD(v=1,2,3) + SO_2 have been studied using a photolysis / laser induced fluorescence technique. The rate coefficients OH/OD(v=1,2,3) + SO_2, k_1, over the temperature range 295 – 810 K were used to determine the limiting high pressure limit, k_1^∞. This method is usually applicable if the reaction samples the potential well of the adduct, $HOSO_2$, and if intramolecular vibrational relaxation is fast. In the present case, however, the rate coefficients showed an additional fast removal contribution as evidenced by the increase in k_1 with vibrational level; this behaviour together with its temperature dependence is consistent with the existence of a weakly bound complex on the potential energy surface prior to adduct formation. The data were analysed using a composite mechanism that incoporates energy transfer mechanisms via both the adduct and the complex, and yielded a value of k_1^∞(295 K) equal to $(7.2 \pm 3.3) \times 10^{-13}$ cm^3 $molecule^{-1}$ s^{-1}, (errors at 1σ) a factor of between two to three smaller than the current recommended IUPAC and JPL values of $(2.0\,^{+2.0}_{-1.0})$ and $(1.6 \pm 0.4) \times 10^{-12}$ cm^3 $molecule^{-1}$ s^{-1} at 298 K, respectively, although the error bars do overlap. k_1^∞ was observed to only depend weakly on temperature. Further evidence for a smaller k_1^∞ is presented in the companion paper.

1. Introduction

Sulphur dioxide (SO_2) is a trace pollutant gas in the Earth's atmosphere. Measurements of atmospheric concentrations of SO_2 suggest that its primary sources are anthropogenic[1] and that it has a relatively short atmospheric lifetime of the order of a few days with respect to reaction with OH. Sulphur released from biogenic sources tends to be in more reduced forms, notably carbonyl sulphide, dimethyl sulphide (DMS) and H_2S.[2-4] The oxidation and interconversion of these species are linked and, while it is estimated that the majority of DMS is converted to SO_2, biogenic sources produce only 10-25% of the total atmospheric load of SO_2.[2, 5-7] The majority of atmospheric SO_2 is directly emitted by human activity and it may have significant environmental impact as it is almost entirely converted to sulphuric acid (H_2SO_4) in the atmosphere, leading to the formation of acid rain[8] as well as particulate formation.[9-10]

As with most atmospheric pollutants, gas phase oxidation of SO_2 by reaction with the OH radical is the main route of chemical removal:

$$OH + SO_2 (+ M) \rightarrow HOSO_2 (+ M) \qquad R1$$

with $HOSO_2$ further reacting with O_2 [11] to form SO_3, which then reacts with H_2O to form H_2SO_4.[12-13] H_2SO_4 leads to aerosol formation and is the major source of new particles in the atmosphere:[14]

$$HOSO_2(g) \xrightarrow{O_2 / H_2O} H_2SO_4(g) \longrightarrow \text{sulphate} \qquad R2$$

Reaction R1 is pressure dependent and is in its falloff regime at atmospheric pressure and below. Its kinetics in this pressure regime have been extensively studied,[15-18] and RRKM modelling of these data have been used to recommend the limiting high-pressure rate coefficient: Wine et al.[18] recommended a value for k_1^∞ between 260 and

420 K equal to 1.3×10^{-12} $(T/300\ K)^{-0.7}$ cm^3 $molecule^{-1}$ s^{-1} and Cobos and Troe [19] recommended $k_1^{\infty} = 2.7 \times 10^{-12} \exp(-80K/T)$ cm^3 $molecule^{-1}$ s^{-1} (k_1^{∞} (300 K) = 2.1×10^{-12} cm^3 $molecule^{-1}$ s^{-1}).

More recently Fulle et al. [20] measured k_1 over an extended pressure range up to 96 bar and their estimate of k_1^{∞} was significantly larger (3.6×10^{-12} cm^3 $molecule^{-1}$ s^{-1} at 300 K) than the above recommendations, and a significant positive activation energy was observed, contrary to the recommendations. Blitz et al.[21] investigated the temperature dependence of k_1^{∞} by monitoring the removal of vibrationally excited hydroxyl radical, OH(v=1), in the presence of SO_2 – the so-called proxy method to measure k_1^{∞} (see below) - and observed a slight negative temperature dependence, where the value of k_1^{∞} $(2.04 \pm 0.10) \times 10^{-12}$ cm^3 $molecule^{-1}$ s^{-1}) was significantly lower than that of Fulle et al., but above the recommendation of Wine et al. IUPAC evaluated the OH + SO_2 reaction in 2012 recommending $k_1^{\infty} = (2.0\ ^{+2.0}_{-1.0}) \times 10^{-12}$ cm^3 $molecule^{-1}$ s^{-1} at room temperature, but with no recommendation on the temperature dependence.[22] The JPL evaluation [23] of this reaction did not consider the Fulle et al. data and assigned a value $k_1^{\infty} = (1.6 \pm 0.4) \times 10^{-12}$ cm^3 $molecule^{-1}$ s^{-1}, slightly lower than the IUPAC value.

In this study, the value for k_1^{∞} and its temperature dependence has been investigated by monitoring the removal of vibrationally excited hydroxyl radical, OH/OD(v=1,2,3), in the presence of SO_2. In our previous study,[21] where only OH(v=1) in the presence of SO_2 was monitored, it was argued that the excited $HOSO_2$ adduct was solely responsible for the removal of OH(v=1), hence giving an estimate of k_1^{∞}.

Assigning the vibrational relaxation rate coefficient as the limiting high-pressure rate coefficient, k^{∞}, of a reaction was first proposed by Jaffer and Smith,[24] and it appears to be valid for reactions that form a reaction collision complex on a long-range attractive surface, i.e. the reaction rate coefficient is independent of vibrational energy. This approach is known as the proxy method and is depicted in Scheme 1 for the reaction R1:

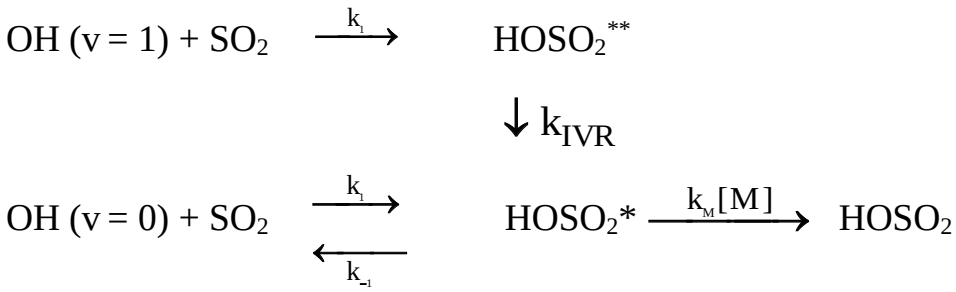

Scheme 1

where $HOSO_2$** represents the adduct prior to intramolecular vibrational relaxation (IVR) and $HOSO_2$* the adduct following IVR. Ergodicity is a central tenet of unimolecular reaction rate theory and appears to be valid for almost all thermal reactions. Re-dissociation of $HOSO_2$**, k_{-1}, occurs mostly to OH (v=0) via $HOSO_2$* so that the removal rate coefficient derived from measurements of OH (v=1), k_1, is a good approximation of the limiting high-pressure rate coefficient, k_1^{∞}. Current understanding indicates occurs via a collision complex on a long-range attractive surface, therefore there is no kinetic isotope effect and k_1^{∞} should be reasonably approximated by:

$$OD + SO_2 (+ M) \rightarrow DOSO_2 (+ M) \qquad R1,D$$

Hence the determination of $k_{1,D}^{\infty}$ provides additional information on R1. Throughout this paper it is assumed that $k_{1,D}^{\infty}$ is equal to k_1^{∞}, even though it is not identical. This method of directly determining the high pressure limiting rate coefficient appears to be

valid for a number of systems, for example OH + NO,[24] and OH + NO_2.[25] In general, as the size of the system increases, the rate of re-dissociation, k_{-1}, decreases[26] and the ergodicity assumption is more readily satisfied. This present study shows that the removal of OH/OD(v=1,2,3) is not solely via the proxy mechanism and there is an additional non-reactive vibrational relaxation contribution via collisions that access a shallower, long range van der Waals well. We show that both contributions can be modelled, and hence are able to assign a more reliable value for k_1^{∞}, that is lower than current recommendations. A detailed consideration of rate coefficient for the reaction of vibrational ground state OH with SO_2, the possible influence of SO_2 photolysis on the kinetics and a comparison of previous literature is presented in the companion paper.

2. Experimental

Laser Flash Photolysis / Laser Induced Fluorescence

The apparatus used to measure the vibrationally excited state OH/OD(v=1,2,3) kinetics is similar to that described previously,[21,27] thus only the salient features are highlighted. An excimer laser (Lambda Physik, LPX 105) was used as the photolysis laser (~ 100 mJ / pulse) for OH/OD (v=1,2,3) generation. The output from an excimer laser (Lambda Physik, LPX 105) pumped dye laser (Lambda Physik, FL2002), was used to monitor OH(v=1,2,3) by off-resonance fluorescence using the dye mixture PTP / DMQ to produce ~ 3 mJ per pulse over the range 345 – 360 nm. OD(v=1,2,3) was probed using the doubled output from a Nd:YAG (Continuum Powerlite 8010) pumped dye laser (Sirah, PrecisionScan, Pyridine 1) system. The laser-excitation scheme used to probe

OH/OD(v) are given in Table 1. The subsequent fluorescence ($A^2\Sigma^+ \rightarrow X^2\Pi_i$) passed through a 308 nm interference filter (Barr Associates), detected using a photomultiplier (Electron Tubes 9813) and the subsequent signal was integrated and digitized on a LeCroy (Waverunner LT372) oscilloscope before being transferred for storage on a PC. Little laser scattered light was observed when detecting species using off-resonant, blue shifted fluorescence schemes. A LabVIEW program controlled the delay generator which scanned the time delay between the photolysis and probe laser, and recorded via the oscilloscope the OH/OD signal. Typically, the time delays were scanned over 200 - 400 points, with each point being the average of up to ten samples. The pulse repetition frequency of the lasers was 5 Hz such that a fresh gas mix was exposed for each photolysis pulse.

The gases were introduced into the reaction cell through a mixing manifold. Control of the gas flows was regulated by mass flow controllers. After the mixing manifold, the gases entered a ten-way cross, stainless steel reaction cell designed for high temperature experiments with a surrounding ceramic fiber heater (Watlow). The pressure in the cell was controlled by throttling the exit valve of the cell and monitored via a capacitance manometer. The total flow was > 10 sccm per Torr total pressure, ensuring that the gases were swept through the cell between laser pulses. The temperature was measured inside the cell by type K thermocouples probing close to the reaction region ensuring temperatures were known to ±5 K. The OH/OD (v=1,2,3) experiments were conducted at a total pressure between 20 - 50 Torr and the temperature was varied over the range 295 – 800 K.

SO_2 was purified by first degassing and then diluted in He. H_2 (Air Products, 99.999) and He (BOC, CP grade 99.999%) were used directly from the cylinder.

OH/OD (v=0,1,2,3) precursors

As in our previous paper [27] vibrationally excited hydroxyl radicals were generated from two photon dissociation of SO_2 at 248 nm to form $O(^1D)$:

$$SO_2 + 2\,h\nu_{248\,nm} \rightarrow O(^1D) + SO \qquad P1$$

followed by the reaction:

$$O(^1D) + H_2 \rightarrow OH(v=0\text{-}4) + H \qquad R3$$

Reaction 3 has been widely studied both experimentally and theoretically[28-30] and is known to produce the following ratios of vibrationally excited OH: v = 1:2:3:4; 0.29: 0.32: 0.25: 0.13.[28] By substituting D_2 for H_2 vibrationally excited OD was produced:

$$O(^1D) + D_2 \rightarrow OD(v=0\text{-}3) + D \qquad R4$$

Typically, the concentration of SO_2 added to the system was $\leq 5 \times 10^{16}$ molecule cm^{-3} and to ensure that the majority of the $O(^1D)$ reacts with hydrogen/deuterium, high concentrations of H_2 or D_2 ($\sim 1 \times 10^{17}$ molecule cm^{-3}) was added to the system. The reaction:

$$OH\ (v=1) + H_2/D_2 \rightarrow OH(v=0) + H_2/D_2 \quad < 1\times10^{-14}\ cm^3\ molecule^{-1}\ s^{-1}\ [31] \qquad R5$$

is relatively slow and is a constant removal process as the H_2/D_2 concentration was kept constant when $[SO_2]$ was varied to determine bimolecular rate coefficients. The reaction H/D + SO_2 to give vibrationally excited hydroxyl does not occur to any significant extent at the temperatures studied here [32] and hence does not affect the removal kinetics of OH/OD(v).

3. Results

OH/OD(v=1,2, 3) + SO_2

Laser excitation spectra of both OH/OD (v=1, 2 and 3) were taken at room temperature and simulated spectra calculated using the LIFBASE[33] program. The experimental values were observed to be in excellent agreement with the calculated line positions. The actual lines used in the experiment are given in Table 1, and were usually the most intense.

The reaction $O(^1D) + H_2$, R3, forms OH in vibrational levels up to OH (v = 4).[28] These high vibrational levels may form sufficiently long-lived collision adducts with SO_2, which result in efficient formation of the ground vibrational state as depicted in Scheme 1:

$$OH\ (v=x) + SO_2 \rightarrow OH\ (v=0) + SO_2 \qquad (k_1^{\infty}) \qquad R1,_{PROXY}$$

or undergo VET via a single step cascade mechanism:

$$OH\ (v=x) + SO_2 \rightarrow OH\ (v=(x-1)) + SO_2 \qquad (k_{VET\ i}) \qquad R1,_{SSH}$$

Theory indicates that VET via a multiple step is much less probable.[34] Provided VET is not close to resonant, this type of cascade mechanism is sufficiently described by the Shin variation of Schwartz, Slawsky and Herzfeld (SSH) theory which incorporates a more realistic form for the intermolecular potential than was used in the original theory.[34-38] In the recent trajectory study by Glowacki et al.[39] the fate of the HO-SO_2 collision adduct was investigated and it was found that the lifetime of the collision adduct was too short to efficiently form the OH ground vibrational state, the statistical limit, as depicted in Scheme 1. However, the dissociation of the adduct resulted mainly in loss of vibrational energy, especially so the higher the initial vibrational level. Therefore the proxy method to determine the limiting high pressure rate coefficient,

k_1^{∞}, should be valid, even though the vibrational levels have not reached the statistical limit, as depicted in Scheme 1.

For the present system both adduct formation and non-reactive vibrational energy transfer (VET), collisions may result in a single step cascade mechanism, hence the OH/OD (v=1,2,3) concentration versus time traces may have significant growth from the higher vibrational levels, and the overall reaction scheme governing the concentration of OH/OD (v=1,2,3) is thus:

$$OH(v=i) + SO_2 \rightarrow OH(v=i-1) + SO_2 \qquad k_{1,i}\ (k_1^{\infty}+k_{VET\,i})$$

$$OH(v=i+1) + SO_2 \rightarrow OH\ (v=i) + SO_2 \qquad k_{1,i+1}\ (k_1^{\infty}+k_{VET\,i+1})$$

where $k_{1,i}$ and $k_{1,i+1}$ are the rate coefficients for both adduct formation and non-reactive VET in OH(v=i) and (v=i+1), respectively, i = 1,2,3. How each component is identified is given in the discussion below, and hence leads to a determination of k_1^{∞}. Glowacki et al.[39] did observe trajectories corresponding to two vibrational quanta jumps via adduct formation but these events were much less significant than single quantum jumps. Therefore the change in concentration of OH/OD (v=1,2,3) is given by the general differential equation:

$$\frac{-d[OH(v=i)]}{dt} = k_{1,i}[SO_2][OH(v=i)]k_i - k_{i+1}[SO_2][OH(v=i+1)] \qquad E1$$

Solution of Equation 1 yields a multi-exponential time dependence for OH/OD(v= 1,2,3),[40] and such behaviour was observed in the present system, see Figure 1.

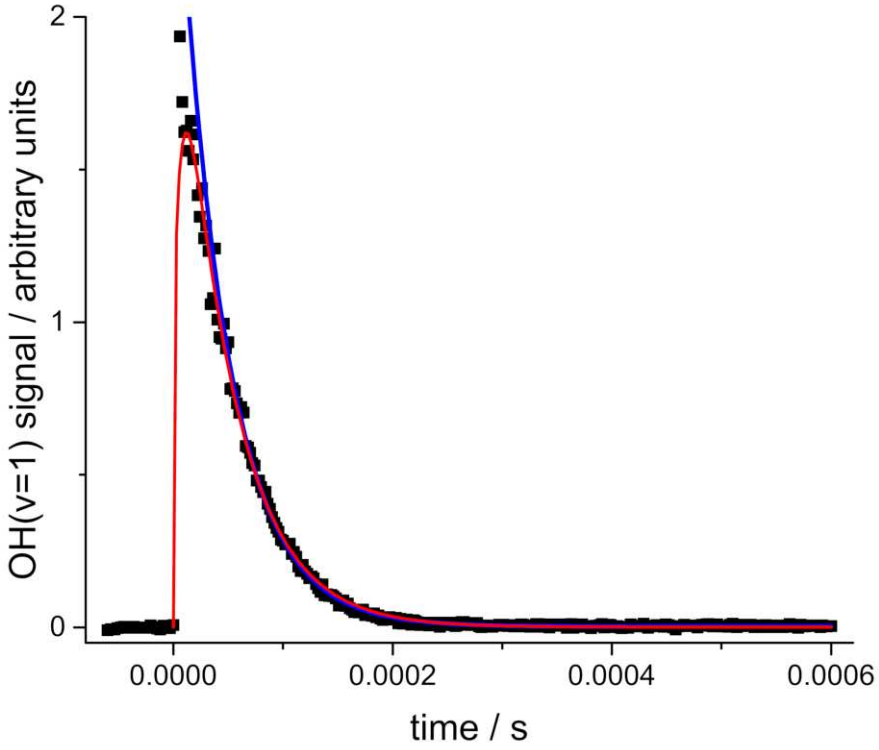

Figure 1. Typical OH(v=1) decay in the presence of SO_2 (1.07×10^{16} molecule cm^{-3}) at 295 K, where filled squares are the measured fluorescence intensities. The total pressure is equal to 37.3 Torr and the added H_2 (6.84×10^{16} molecule cm^{-3}) ensures that the $O(^1D)$ is titrated to OH(v). The lines are a biexponential (red) and (from t=50 μs) exponential (blue) fit to the data, where the decay rate coefficients are (2.69 ± 0.39) and (2.29 ± 0.02) $\times 10^4$ s^{-1}, respectively. Note that the red and blue lines converge and this is the point where the culled exponential analysis is carried out (see text for details).

For any given vibrational level, the full solution involves growth from more than one higher vibrational level; hence the analytical solution is complicated. In addition, if there is growth from multiple quanta jumps – Glowacki et al. showed that this occurs [39] – then the solution becomes intractable even when the initial vibrational populations are known. An approximate solution is to treat it as a two level system: growth from above is lumped together and loss from the probed vibrational level. This leads to an analytical biexponential solution, and an example of fitting this to the data is shown in Figure 1. While this equation provides a good fit to the data, the returned

loss rate coefficient from the probed level often had large errors, especially when its values were close to the growth rate coefficient from the higher vibrational levels. Although constraints could be applied to improve the errors on the returned rate coefficient, a more systematic and easier approach is to fit the OH/OD(v=1,2,3) data to a single exponential decay given by:

$$[\mathrm{OH/D(v=1,2,3)}]_t = [\mathrm{OH/D(v=1,2,3)}]_0 e^{-k_{obs}t} \qquad \text{E2}$$

where $k_{obs} = k_i [SO_2] + k_{other}$, $k_i = (k_1^{\infty} + k_{VET\ i})$ and k_{other} is the pseudo first order rate coefficient for loss of these states by other routes. Contributions from growth in OH/OD(v=1,2,3) are revealed as a decrease in the observed pseudo-first-order rate coefficient, k_{obs}.[40] To minimise this contribution, individual points were sequentially culled starting from t = 0, the decay trace recalculated and this procedure repeated until there was no increase in the fitted rate coefficient, see Figure 1. In our previous paper on OH + C_2H_2[27] we carried out simulations and determined that the error in the observed rate coefficient from using equation E2 was ~ 10 - 15% of the actual rate coefficient entered into the numerical model. This is in agreement with the cascade analysis carried out by Silvente et al.[40] In Figure 2 the returned $k_i[SO_2]$ parameters versus $[SO_2]$ are plotted from analysis of the OH(v=1) + SO_2 at 295 K data using the biexponential equation and a single exponential, E2.

Both biexponential analysis (E1) and culled exponential (E2) analysis returned rate coefficients in close agreement, but both analyses are potentially prone to systematic errors, so it is difficult to indicate which returns the most accurate rate coefficients. As culled exponential analysis is more straightforward to apply, we have used this for the majority of the data analysis. Therefore, while it is acknowledged that

the returned values for k_i are potentially skewed, it is reasonable to expect that these values are affected in a similar way. It is estimated that this skewing of the data is no greater than ±15%, hence a ±15% error was added to k_i. Analysis of the OH(v=1) + SO_2 at 295 K data using equation E1 is shown in Figure 1.

From analysis of all the vibrational levels (see Table 2) it was evident that k_i increased strongly with i, which has been previously observed in OH(v=1,2) + C_2H_2 [27] and indicates that non-reactive VET is the major component of the removal process. Therefore the growth rate coefficient is faster than the loss rate coefficient, hence the OH(v=i) trace better approximates a single exponential with a pseudo-first rate coefficient $k_i[SO_2]$ at later times. In Figure 1 it can be seen that after ca. one half-life the data are a good approximation to a single exponential (blue line).

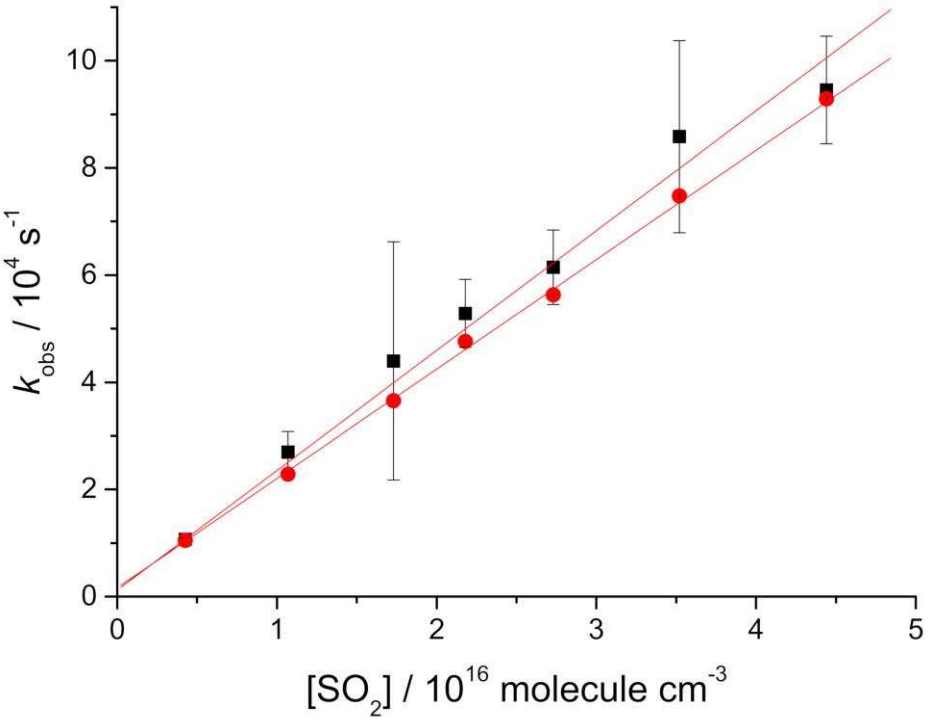

Figure 2. Typical bimolecular plot for OH(v=1) at 295 K, ~ 40 Torr total pressure of He, where the squares and circles are obtained from equations E1 ($k_i[SO_2] = k_{obs}$) and E2, respectively, and linear regression gives bimolecular rate coefficient of (2.24 ± 0.16) and (2.04 ± 0.01) × 10^{-12} cm^3 $molecule^{-1}$ s^{-1}, respectively.

The fitted rate coefficient, k_{obs}, was measured over a range of sulphur dioxide concentrations. The concentration of added H_2/D_2 was always greater than the highest SO_2 concentration, ~5×10^{16} molecule cm^{-3}, and the total pressure was typically ~40 Torr. The gradient of k_{obs} vs. $[SO_2]$ graph is the bimolecular rate coefficient k_i. Typical plots of k_{obs} against $[SO_2]$ are shown in Figure 2 along with the best straight-line fit to the data, via linear regression. Bimolecular rate coefficients were measured at temperatures between 295 K and 810 K and the results are shown in Tables 2 and 3.

All the results are summarized in Table 2 and 3 (OH/OD(v=1,2,3)) and plotted in Figures 3 and 4. From Table 2 and Figure 3, it is clear that the value $k_1^{\infty} = 3.6 \times 10^{-12}$ cm^3 $molecule^{-1}$ s^{-1} determined from the measurements of Fulle et al.[20] at 295 K is too high. This most likely arises from SO_2 photolysis, see the companion paper.

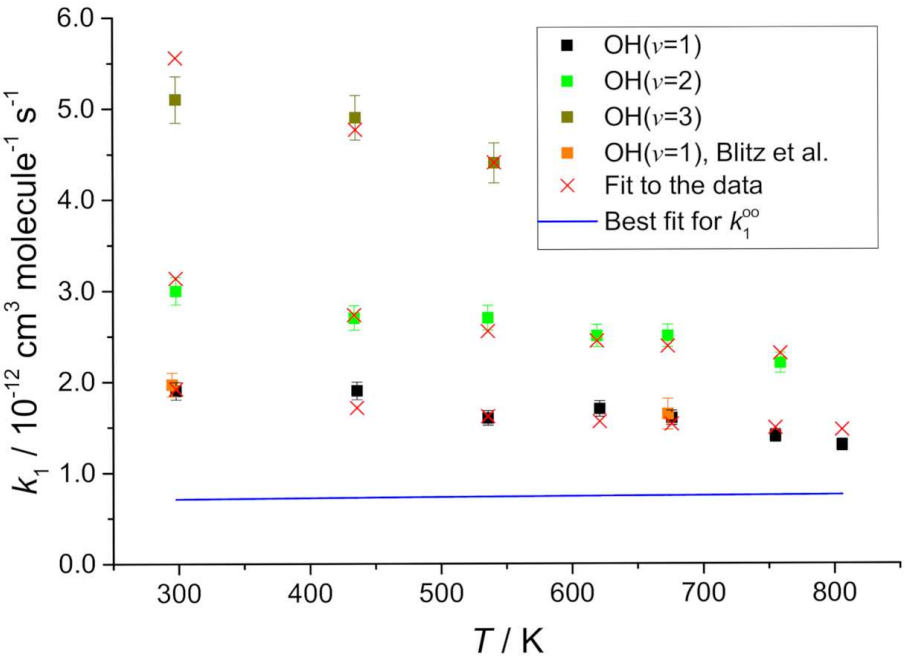

Figure 3. OH(v=1,2,3) + SO_2 data fitted to composite function that accounts for complex formation and non-reactive VET, SSH-type. The symbols are the data, which includes Blitz et al.,[21] and the red crosses are the best fit (Equation 4, see Table 4 for the fitting parameters). These fitting parameters predict k_1^{∞} = (7.1 ± 3.3) × 10^{-13} × (T/298)$^{0.06}$ cm^3 $molecule^{-1}$ s^{-1}, the blue line.

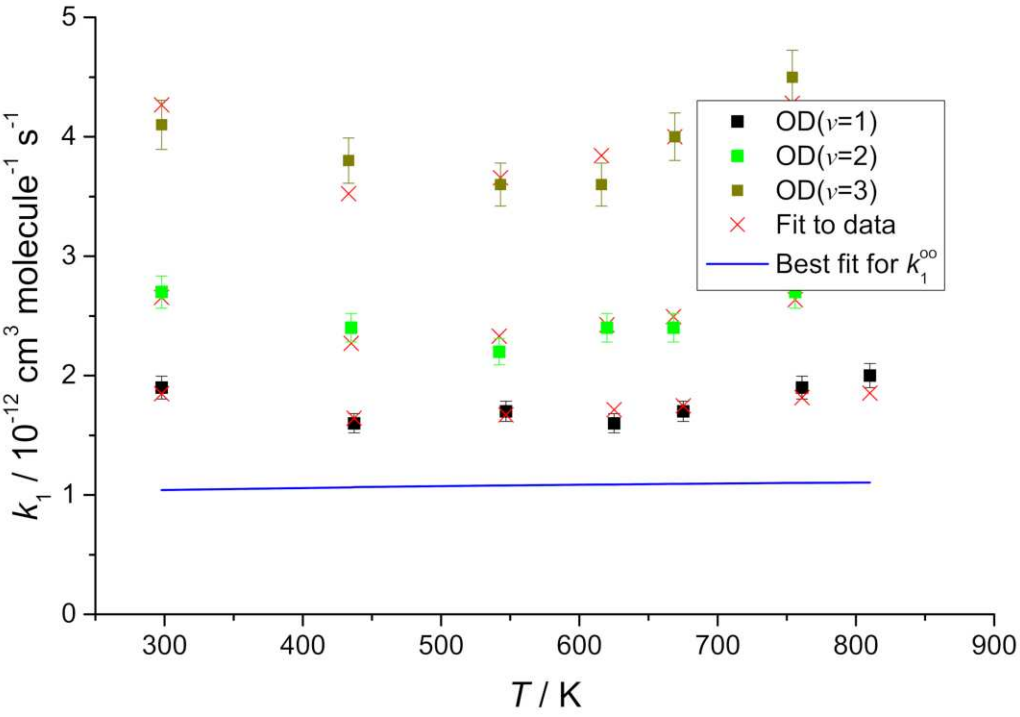

Figure 4. OD(v=1,2,3) + SO_2 data fitted to composite function that accounts for complex formation and non-reactive VET, SSH-type. The symbols are the data and the red crosses are the best fit (Equation 4, see Table 4 for the fitting parameters). These fitting parameters predict $k_1^{\infty} = (10.4 \pm 2.5) \times 10^{-13} \times (T/298)^{0.06}$ cm^3 $molecule^{-1}$ s^{-1}, the blue line.

4. Discussion

Interpretation of the results for OH/OD(v=1,2,3)

The results from these experiments show that the rate coefficients, k_i, for the removal of OH/OD(v=1,2,3) by SO_2 (Figures 3 and 4) increase with increasing vibrational level, i. This means that the system is more complicated than removal by adduct formation, i.e. the proxy method as depicted in Scheme 1. In our previous study on reaction R1, [21] only OH(v=1) + SO_2 was studied and it was assumed that only the proxy method was operating and $k_1^{\infty} = 2.0 \times 10^{-12}$ cm^3 $molecule^{-1}$ s^{-1} was assigned. The present findings

indicate that this value is an overestimate of k_1^{∞} as the increase in k_i with vibrational level means that there is a contribution from non-reactive VET. This increase of k_i on vibrational level was previously observed in our study on OH(v =1,2) + C_2H_2,[27] where it was concluded that a weakly bound, van der Waals, vdW, complex facilitates an additional route for loss of vibrational energy. This weakly bound complex is too short lived at the temperatures of these experiments for efficient intramolecular energy redistribution and VET is better described by an extended form of SSH theory developed by Shin.[34-38] The weakly bound adduct between OH + C_2H_2 is ~ 10 kJ mol^{-1} [41-42] but no such adduct has been observed or predicted between OH + SO_2. To explain the present results a weakly bound complex needs to be invoked, and its presence also provides explanation of why k_1^{∞} is so small, something that is hard to rationalise if HO-SO_2 is formed on a simple barrierless potential energy surface, PES. The trajectory calculations by Glowacki et al.[39] were carried on a simple, barrierless, analytical PES that started with a vibrationally excited HO-SO_2 chemically bound adduct and followed its progression to OH + SO_2; no vdW complex was included on this PES. Therefore the results from this calculation are only applicable for vibrational energy transfer from the HO-SO_2 adduct and not from the vdW complex, which is the major loss route in the system.

The OH/OD(ν=1,2,3) + SO_2 data in Figures 3 and 4, respectively, show that each increase in the vibrational level results in a significant increase in k_i, but this increase is less than if VET were assumed to conform to SSH theory: [34]

$$k_{VET\,i} = k_{VET\,1} \times 2^{i-1} \qquad \text{E3}$$

This indicates that vibrational energy removal via the proxy mechanism is making a significant contribution to k_i. Over the range 300 - 500 K, k_i shows a small but discernible decrease, and the OD data, which appears to be of higher quality than the OH data – the SO_2 photolysis products produced a background signal that was subtracted away – above 500 K increases to a small extent. This temperature dependence is subtle compared to OH(v=1,2) + C_2H_2 where a distinct minimum was observed at ~ 300 K, with k_i increasing much more strongly with temperature. This higher temperature minimum for OH(D)/SO_2 implies that its vdW complex is slightly more strongly bound than that between OH/C_2H_2, ~ 10 kJ mol^{-1}, [41-42] based on the observation that the probability for VET in HCl and HF was seen to go through a minimum at ca. 350 and 1000 K, respectively, where the heats of dimerization are 9 and 25 kJ mol^{-1}, respectively.[34]

The theory of non-reactive vibrational energy transfer is based on the original theoretical work by Schwartz, Slawsky and Herzfeld (SSH) who developed a model for vibration to translation energy transfer on a repulsive potential and demonstrated that the rate coefficient increases with temperature according to the relationship ln $k \propto 1/T^{1/3}$.[34] The model was further developed by Shin to include an attractive component to the potential and demonstrated that an inverse temperature dependence of the rate coefficient occurs at low temperature, where ln $k \propto 1/T^2$. [34-37] Shin constructed his analysis on dipole - dipole or dipole – quadrupole interactions and used this model to explain the irregular temperature dependence of vibrational energy transfer for HF with several other encounter molecules (e.g. DF, HF and CO_2). In our previous paper on OH + C_2H_2, the data were analysed by using an expression that accommodates removal of

vibrational energy via both the vdW complex, extended SHH, and the HO-SO_2 adduct, the proxy method, and the rate coefficient is given by:

$$k_{VETi} = B\left[\exp^{\left(\frac{C}{T^{1/3}}+\frac{D}{T^2}\right)}\right] n^{i-1} + A(T/295)^E \qquad \text{E4}$$

where $k_{VETv\,i}$ is the overall bimolecular rate coefficient for loss of OH/OD in (i=1,2,3), B, C, D are the SSH parameters and A and E are the parameters describing the high pressure limit for reaction R1, k_1^∞. The parameter n describes the enhancement of the rate coefficient for non-reactive VET with increasing vibrational quantum number and n was explored during the analysis; for a harmonic oscillator, n = 2.

Equation E4 was used to fit the OH and OD(v=1,2,3) + SO_2 rate coefficient data, where T and v were the two independent variables and the data were weighted to the uncertainty in $k_{VET,\,I}$, weight $\propto 1/\sigma^2$. A non-linear least-square fitting routine was used to locate the best-fit parameters, and the resulting fit is shown in Figures 3 and 4, and the returned parameters and uncertainties are given in Table 4. From Figures 3 and 4 it can be seen that Equation E4 is a good fit to both the OH and OD (v=1, 2 and 3) + SO_2 data. There are no vibrations or combinations in SO_2 that lie within 30 cm^{-1} of the OH stretch, so energy transfer is expected to be non-resonant and adequately described by the left hand terms of equation E4. However, the interpretation of the non-reactive VET B, C and D parameters is beyond the scope of this analysis.

In the analysis the value of n was constrained such that $n \geq 2.0$, the harmonic limit. It is noted that in this analysis the uncertainties in the non-reactive VET parameters (Table 4) are considerably larger than $k_1^\infty(T)$. Table 4 gives the values for k_1^∞ for both OH and OD + SO_2, where k_1^∞ is observed to only have a weak, slightly

positive dependence on temperature. As noted above, the OD data were of better quality than the OH data and all the fitting parameters were allowed to float, see Table 4. For the OH data the temperature dependence of k_1^∞ - E in Table 4 - was fixed to the same value as OD and the value of D was not allowed to be negative; this ensures that non-reactive VET increases at low T, as is the case for OD and OH + C_2H_2.[27] The OD(v)/SO_2 data points to a similar value for the limiting high-pressure rate coefficient, $k_{1(D)}^\infty$, for

$$OD + SO_2 (+M) \rightarrow DOSO_2 (+ M) \qquad R1(D)$$

which reinforces the current assignment, but it is not clear if they should be the same due the uncertain impact of the pre-reaction complex.

General Discussion

From Figure 3, the OH(v=1,2,3) + SO_2 data show a distinct dependence on the vibrational level, v, therefore the value of k_1^∞ in our previous work,[21] where we assigned k_1^∞ equal to k(OH(v=1) + SO_2), is an overestimate (n.b. the absolute rate coefficient for OH(v=1) removal we previously determined is in excellent agreement with the present work, see Figure 3). Figure 3 indicates that OH(v) removal by SO_2 is mainly by energy transfer in collisions that do not sample the deep $HOSO_2$ well (SSH-type behaviour), in contrast to vibrational relaxation via the proxy mechanism where relaxation occurs following IVR in the deep well. In the present case, the latter is minor but is being identified in our analysis in order to assign k_1^∞. Analysis via equation E4 reinforced this observation and assigned a value $k_1^\infty = (7.2 \pm 3.3) \times 10^{-13}$ cm^3 molecule^{-1} s^{-1}. Therefore the OH(v=1,2,3) + SO_2 data indicate that the value of k_1^∞(T) is smaller than both the IUPAC and JPL recommendations: ($2.0\ ^{+2.0}_{-1.0}$) and $(1.6 \pm 0.4) \times 10^{-12}$ cm^3 molecule^{-1} s^{-1}, respectively.[22-23] This low value for k_1^∞ is supported in the companion paper where all

the literature values for OH(v=0) + SO_2 measurements, together with some new measurements, are analysed using a master equation. However, it is noted that if the D parameter, which increases the rate coefficient as temperature is lowered, is floated with a lower bound equal to 1.5×10^5, the value obtained for OD(v=1,2,3) + SO_2, this returns a value $k_1^\infty = (11.5 \pm 3.6) \times 10^{-13}$ cm^3 molecule^{-1} s^{-1}, see Table 4. This value represents an upper limit to k_1^∞ and is obtained when the fit to the data is ~ 3 times worse, see Table 4.

The implication from the OH(v) + SO_2 rate coefficient data is that a pre-reaction, weakly bound complex is the main channel for OH(v) removal, hence the use of equation, E4, in assigning the limit high-pressure rate coefficient, k_1^∞. To date, no ab initio calculation has observed such a weakly bound complex, OH—OSO.[43-44] This suggestion links to the reaction between OH + NO_2 where the weakly bound HOONO complex was only identified in the last decade because of the inconsistencies in the rate coefficients if OH + NO_2 was just forming $HONO_2$.[45-50] The HOONO intermediate is bound by ~100 kJ mol^{-1} [49] and affects the OH + NO_2 kinetics at room temperature. But this OH—OSO complex is estimated – see above – to be bound by < 20 kJ mol^{-1}, which is too weakly bound to influence the kinetics at room temperature. The binding energy of the adduct between OH and CH_3OH is ~ 20 kJ mol^{-1} [51] and in recent work at Leeds it has been demonstrated that it is only below 170 K that the adduct significantly influences the observed kinetics.[52] Therefore it is mainly the OH(v) + SO_2 kinetics that points to the presence of OH—OSO but it does provide explanation of why k_1^∞ is so small and exhibits little temperature dependence. If the reaction were on a barrierless potential energy surface, k_1^∞ would be expected to be fast and if there was a significant barrier (to explain the low value of k_1^∞), then a positive temperature dependence should

be observed; OH + SO_2 exhibits neither of these properties. This contradiction is removed if the reaction occurs via a pre-reaction complex as depicted in Figure 5.

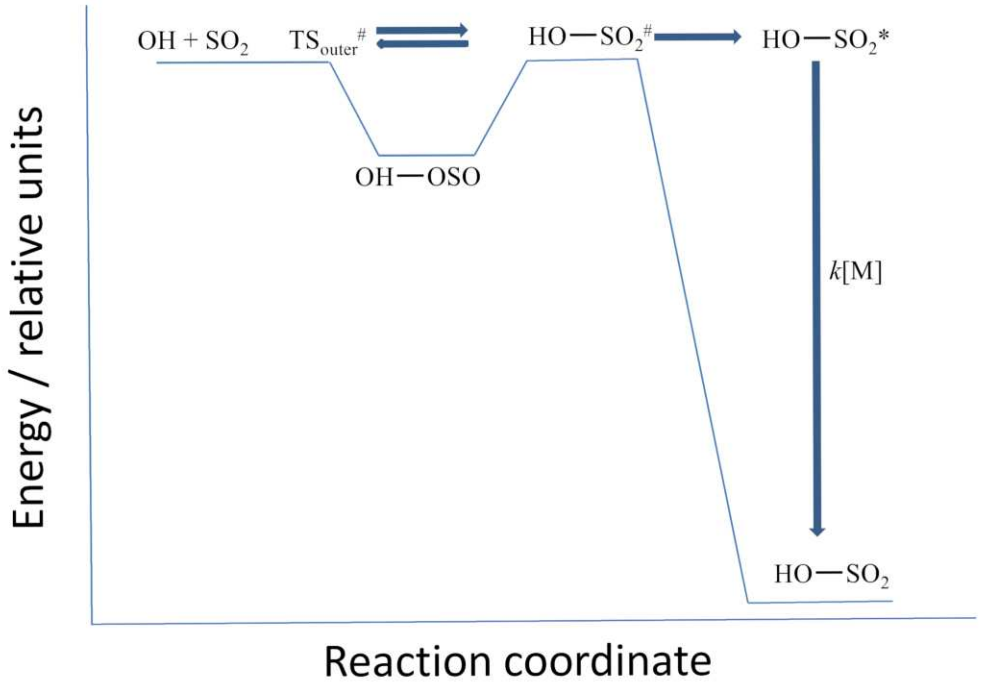

Figure 5. A qualitative potential energy surface for the reaction between OH + SO_2 based on the findings from this study, where a weakly bound complex, OH-OSO, is initially formed before proceeding to product, HO-SO_2.

This type of potential energy surface has been discussed in our recent paper on OH + CH_3OH [52] and it implies that the measured rate coefficient is a mixture of complex formation and further reaction to products. The PES predicts a fast removal at low temperatures, $TS_{outer}^{\#}$ controlled, and at high temperatures it is controlled by the barrier associated with HO—$SO_2^{\#}$. If at room temperature the rate coefficient was controlled exclusively by HO—$SO_2^{\#}$ then it would be reasonable to expect that OH + SO_2 ($k_{1,H}^{\infty}$ = (7.2 ± 3.3) × 10^{-13} cm^3 $molecule^{-1}$ s^{-1}) and OD + SO_2 ($k_{1,D}^{\infty}$ = (10.4 ± 2.5)

$\times 10^{-13}$ cm^3 $molecule^{-1}$ s^{-1}) to be similar, and this appears to be the case. But it is noted at room temperature, if $TS_{outer}^{\#}$ is still influencing the rate coefficient then the higher density of states of OD—OSO compared to OH—OSO will increase k_1^{∞}. By analogy to OH + CH_3OH, at room temperature the inner TS is controlling the rate coefficient, but not exclusively.

6. Conclusions and summary

(i) The rate coefficients for the removal OH/OD(v=1,2,3) by SO_2 have been studied as a function of temperature (295 – 810 K) using laser flash photolysis coupled with laser induced fluorescence. The dependence of the rate coefficients on temperature and on vibrational quantum number demonstrate that there is a significant contribution from what has been termed non-reactive vibrational relaxation, which is attributed to the van der Waals complex OH—OSO. This is the first speculation on the existence of OH—OSO, which is too weakly bound to allow significant energy redistribution, leading to incomplete IVR.

(ii) OH—OSO is mainly responsible for the observed temperature behaviour, which is typical of cascade ($\Delta v=-1$) vibrational relaxation influenced by the attractive van der Waals interaction and by the repulsive wall of the interaction potential.

(iii) Analysis of the data using a mechanism that includes both incomplete IVR, OH—OSO, and complete IVR involving the formation of the chemically bound HO-SO_2 adduct allows k_1^{∞}, the high pressure limiting rate coefficient for formation of the adduct, to be determined.

(iv) The data show systematically lower values for k_1^{∞} ($k_{1,H}^{\infty} = (7.2 \pm 3.3) \times 10^{-13}$ and $k_{1,D}^{\infty} = (10.4 \pm 2.5) \times 10^{-13}$ cm^3 $molecule^{-1}$ s^{-1}) than is currently recommended by

both IUPAC and JPL, ($2.0^{+2.0}_{-1.0}$) and $(1.6 \pm 0.4) \times 10^{-12}$ cm^3 $molecule^{-1}$ s^{-1}, and in even larger disagreement with the values for k_1^{∞} reported by Fulle et al. using high pressure techniques, which could be biased by not accounting for SO_2 photolysis.

(v) In the companion paper, further evidence for a significantly smaller k_1^{∞} is explored by characterising SO_2 photolysis, determining $k_1(p)$ and master equation analysis.

Acknowledgements

We thank Mike Pilling for providing helpful discussions and proof reading this manuscript. We are grateful to NERC (NE/K005820/1) and EPSRC (GR/T28560/01) for funding.

References

1. Thornton, D. C.; Bandy, A. R.; Blomquist, B. W.; Driedger, A. R.; Wade, T. P. Sulfur Dioxide Distribution over the Pacific Ocean 1991-1996. J. Geophys. Res., [Atmos.] **1999,** 104, 5845-5854.
2. Bates, T. S.; Lamb, B. K.; Guenther, A.; Dignon, J.; Stoiber, R. E. Sulfur Emissions to the Atmosphere from Natural Sources. J. Atmos. Chem. **1992,** 14, 315-337.
3. Leck, C.; Rodhe, H. Emissions of Marine Biogenic Sulfur to the Atmosphere of Northern Europe. J. Atmos. Chem. **1991,** 12, 63-86.
4. Turner, S. M.; Liss, P. S. Measurements of Various Sulfur Gases in a Coastal Marine Environment. J. Atmos. Chem. **1985,** 2, 223-232.
5. Benkovitz, C. M.; Berkowitz, C. M.; Easter, R. C.; Nemesure, S.; Wagener, R.; Schwartz, S. E. Sulfate Over the North Atlantic and Adjacent Continental Regions: Evaluation for October and November 1986 Using a Three-Dimensional Model Driven by Observation-Derived Meteorology. J. Geophys. Res., [Atmos.] **1994,** 99, 20725-20756.
6. Benkovitz, C. M.; Scholtz, M. T.; Pacyna, J.; Tarrason, L.; Dignon, J.; Voldner, E. C.; Spiro, P. A.; Logan, J. A.; Graedel, T. E. Global Gridded Inventories of Anthropogenic Emissions of Sulfur and Nitrogen. J. Geophys. Res., [Atmos.] **1996,** 101, 29239-29253.
7. Langner, J.; Rodhe, H. A Global Three-Dimensional Model of the Tropospheric Sulfur Cycle. J. Atmos. Chem. **1991,** 13, 225-263.
8. Calvert, J. G.; Lazrus, A.; Kok, G. L.; Heikes, B. G.; Walega, J. G.; Lind, J.; Cantrell, C. A. Chemical Mechanisms of Acid Generation in the Troposphere. Nature (London) **1985,** 317, 27-35.
9. Fowler, D.; Pilegaard, K.; Sutton, M. A.; Ambus, P.; Raivonen, M.; Duyzer, J.; Simpson, D.; Fagerli, H.; Fuzzi, S.; Schjoerring, J. K.; et al. Atmospheric composition change: Ecosystems-Atmosphere interactions. Atmos. Environ. **2009,** 43, 5193-5267.
10. Wesely, M. L.; Cook, D. R.; Hart, R. L.; Speer, R. E. Measurements and Parameterization of Particulate Sulfur Dry Deposition over Grass. J. Geophys. Res., D: Atmos. **1985,** 90, 2131-2143.
11. Stockwell, W. R.; Calvert, J. G. The Mechanism of the Hydroxyl-Sulfur Dioxide Reaction. Atmos. Environ. **1983,** 17, 2231-2235.
12. Lovejoy, E. R.; Hanson, D. R.; Huey, L. G. Kinetics and Products of the Gas-Phase Reaction of SO_3 with Water. J. Phys. Chem. **1996,** 100, 19911-19916.
13. Reiner, T.; Arnold, F. Stratospheric SO_3: Upper Limits Inferred from Ion Composition Measurements - Implications for H_2SO_4 and Aerosol Formation. Geophys. Res. Lett. **1997,** 24, 1751-1754.
14. Carslaw, K. S.; Lee, L. A.; Reddington, C. L.; Mann, G. W.; Pringle, K. J. The Magnitude and Sources of Uncertainty in Global Aerosol. Faraday Disc. **2013,** 165, 495-512.
15. Lee, Y. Y.; Kao, W. C.; Lee, Y. P. Kinetics of the Reaction Hydroxyl + Sulfur Dioxide in Helium, Nitrogen, and Oxygen at Low Pressure. J. Phys. Chem. **1990,** 94, 4535-4540.

16. Martin, D.; Jourdain, J. L.; G., L. B. Discharge Flow Measurements of the Rate Constants for the Reaction OH + SO_2 + He and $HOSO_2$ + O_2 in Relation with the Atmospheric Oxidation of Sulfur Dioxide. J. Phys. Chem. **1986,** 90, 4143-4147.
17. Paraskevopoulos, G.; Singleton, D. L.; Irwin, R. S. Rates of Hydroxyl Radical Reactions. The Reaction Hydroxyl Radical + Sulfur Dioxide + Molecular Nitrogen. Chem. Phys. Lett. **1983,** 100, 83-87.
18. Wine, P. H.; Thompson, R. J.; Ravishankara, A. R.; Semmes, D. H.; Gump, C. A.; Torabi, A.; Nicovich, J. M. Kinetics of the Reaction OH + SO_2 + M → $HOSO_2$ + M. Temperature and Pressure Dependence in the Fall-Off Region. J. Phys. Chem. **1984,** 88, 2095-2104.
19. Cobos, C. J.; Troe, J. Theory of Thermal Unimolecular Reactions at High Pressures. II. Analysis of Experimental Results. J. Chem. Phys. **1985,** 83, 1010-1015.
20. Fulle, D.; Hamann, H. F.; Hippler, H. The Pressure and Temperature Dependence of the Recombination Reaction HO + SO_2 + M → $HOSO_2$ + M. Phys. Chem. Chem. Phys. **1999,** 1, 2695-2702.
21. Blitz, M. A.; Hughes, K. J.; Pilling, M. J. Determination of the High-Pressure Limiting Rate Coefficient and the Enthalpy of Reaction for OH + SO_2. J. Phys. Chem. A **2003,** 107, 1971-1978.
22. Atkinson, R.; Baulch, D. L.; Cox, R. A.; Crowley, J. N.; Hampson, R. F.; Hynes, R. G.; Jenkin, M. E.; Rossi, M. J.; Troe, J. Evaluated Kinetic and Photochemical Data for Atmospheric Chemistry: Volume I - Gas Phase Reactions of Ox, HOx, NOx and SOx Species. Atmos. Chem. Phys. **2004,** 4, 1461-1738.
23. Burkholder, J. B.; Sander, S. P.; Abbatt, J.; Barker, J. R.; Huie, R. E.; Kolb, C. E.; Kurylo, M. J.; Orkin, V. L.; Wilmouth, D. M.; Wine, P. H. "Chemical Kinetics and Photochemical Data for Use in Atmospheric Studies, Evaluation No. 18," JPL Publication 15-10, Jet Propulsion Laboratory, Pasadena. 2015 http://jpldataeval.jpl.nasa.gov.
24. Jaffer, D. H.; Smith, I. W. M. Time-Resolved Measurements on the Relaxation of OH(v = 1) by NO, NO_2 AND O_2. Faraday Disc. **1979,** 67, 212-220.
25. D'Ottone, L.; Bauer, D.; Campuzano-Jost, P.; Fardy, M.; Hynes, A. J. Kinetic and Mechanistic Studies of the Recombination of OH with NO2: Vibrational Deactivation, Isotopic Scrambling and Product Isomer Branching Ratios. Faraday Disc. **2005,** 130, 111-123.
26. Smith, I. W. M. The Collision Dynamics of Vibrationally Excited Molecules. Chem. Soc. Rev. **1985,** 14, 141-60.
27. McKee, K. W.; Blitz, M. A.; Cleary, P. A.; Glowacki, D. R.; Pilling, M. J.; Seakins, P. W.; Wang, L. Experimental and Master Equation Study of the Kinetics of OH + C_2H_2: Temperature Dependence of the Limiting High Pressure and Pressure Dependent Rate Coefficients. J. Phys. Chem. A **2007,** 111, 4043-4055.
28. Aker, P. M.; Sloan, J. J. The Initial Product Vibrational-Energy Distribution in the Reaction between O(^{1}D) and H_2. J. Chem. Phys. **1986,** 85, 1412-1417.
29. Alagia, M.; Balucani, N.; Cartechini, L.; Casavecchia, P.; van Kleef, E. H.; Volpi, G. G.; Kuntz, P. J.; Sloan, J. J. Crossed Molecular Beams and Quasiclassical Trajectory Studies of the Reaction O(^{1}D)+H_2(D_2). J. Chem. Phys. **1998,** 108, 6698-6708.
30. Dai, J. Q. Quantum state-resolved dynamics study for the reaction O(^{1}D)+H_2->OH+H(J=0). J. Chem. Phys. **1997,** 107, 4934-4942.
31. Rensberger, K. J.; Jeffries, J. B.; Crosley, D. R. Vibrational-Relaxation of OH(CHI-2-PI-I, v=2). J. Chem. Phys. **1989,** 90, 2174-2181.

32. Blitz, M. A.; Hughes, K. J.; Pilling, M. J.; Robertson, S. H. Combined Experimental and Master Equation Investigation of the Multiwell Reaction H + SO_2. J. Phys. Chem. A **2006,** 110, 2996-3009.
33. Luque, J.; Crosley, D. R. LIFBASE: Database and Spectral Simulation Program, 1.5; SRI International Report MP 99-009: 1999.
34. Lambert, J. D. Vibrational and Rotational Relaxation in Gases. Clarendon Press: Oxford, 1978.
35. Shin, H. K. Temperature Dependence of Intermolecular Energy Transfer in Polar Molecules. J. Am. Chem. Soc. **1968,** 90, 3029-3039.
36. Shin, H. K. Vibrational-Rotational-Translational Energy Transfer in HF-HF and DF-DF. Chem. Phys. Letts. **1971,** 10, 81-85.
37. Shin, H. K. Deexcitation of Molecular Vibrations on Collision: Vibration to Rotation Energy Transfer in Hydrogen Halides. J. Phys. Chem. **1971,** 75, 1079-1090.
38. Shin, H. K. Temperature Dependence of V - R,T Energy Transfer Probabilities in CO_2(0,0,1) + HF/DF. J. Chem. Phys. **1974,** 60, 2167-2168.
39. Glowacki, D. R.; Reed, S. K.; Pilling, M. J.; Shalashilin, D. V.; Martinez-Nunez, E. Classical, Quantum and Statistical Simulations of Vibrationally Excited $HOSO_2$: IVR, Dissociation, and Implications for OH + SO_2 Kinetics at High Pressures. Phys. Chem. Chem. Phys. **2009,** 11, 963-974.
40. Silvente, E.; Richter, R. C.; Hynes, A. J. Kinetics of the Vibrational Deactivation of OH X($^2\Pi$)(v=3, 2, 1) with Hydrides and Reduced Sulfides. J. Chem. Soc., Faraday Trans. **1997,** 93, 2821-2830.
41. Davey, J. B.; Greenslade, M. E.; Marshall, M. D.; Lester, M. I.; Wheeler, M. D. Infrared Spectrum and Stability of a PI-type Hydrogen-Bonded Complex between the OH and C_2H_2 Reactants. J. Chem. Phys. **2004,** 121, 3009-3018.
42. Senosiain, J. P.; Klippenstein, S. J.; Miller, J. A. The Reaction of Acetylene with Hydroxyl Radicals. J. Phys. Chem. A **2005,** 109, 6045-6055.
43. Somnitz, H. Quantum Chemical and Dynamical Characterization of the Reaction OH + SO_2 = $HOSO_2$ over an Extended Range of Temperature and Pressure. Phys. Chem. Chem. Phys. **2004,** 6, 3844-3851.
44. Klopper, W.; Tew, D. P.; Gonzalez-Garcia, N.; Olzmann, M. Heat of Formation of the $HOSO_2$ Radical from Accurate Quantum Chemical Calculations. J. Chem. Phys. **2008,** 129, 114308/1-114308/7.
45. Bean, B. D.; Mollner, A. K.; Nizkorodov, S. A.; Nair, G.; Okumura, M.; Sander, S. P.; Peterson, K. A.; Francisco, J. S. Cavity Ringdown Spectroscopy of cis-cis HOONO and the HOONO/$HONO_2$ Branching Ratio in the Reaction OH+NO_2+M. J. Phys. Chem. A **2003,** 107, 6974-6985.
46. Fry, J. L.; Nizkorodov, S. A.; Okumura, M.; Roehl, C. M.; Francisco, J. S.; Wennberg, P. O. Cis-cis and trans-perp HOONO: Action Spectroscopy and Isomerization Kinetics. J. Chem. Phys. **2004,** 121, 1432-1448.
47. Golden, D. M.; Barker, J. R.; Lohr, L. L. Master Equation Models for the Pressure- and Temperature-Dependant Reactions HO+NO_2 → $HONO_2$ and HO+NO_2 → HOONO. J. Phys. Chem. A **2003,** 107, 11057-11071.
48. Hippler, H.; Krasteva, N.; Nasterlack, S.; Striebel, F. Reaction of OH+NO_2: High Pressure Experiments and Falloff Analysis. J. Phys. Chem. A **2006,** 110, 6781-6788.
49. Zhang, J. Y.; Donahue, N. M. Constraining the Mechanism and Kinetics of OH+NO_2 and HO_2+NO using the Multiple-Well Master Equation. J. Phys. Chem. A **2006,** 110, 6898-6911.

50. Zhang, X.; Nimlos, M. R.; Ellison, G. B.; Varner, M. E.; Stanton, J. F. Infrared Absorption Spectra of Matrix-Isolated cis, cis-HOONO and its ab initio CCSD(T) Anharmonic Vibrational Bands. J. Chem. Phys. **2006,** 124, 084305/1-084305/7.
51. Xu, S.; Lin, M. C. Theoretical Study on the Kinetics for OH Reactions with CH_3OH and C_2H_5OH. Proc. Combust. Inst. **2007,** 31, 159-166.
52. Shannon, R. J.; Blitz, M. A.; Goddard, A.; Heard, D. E. Accelerated Chemistry in the Reaction between the Hydroxyl Radical and Methanol at Interstellar Temperatures Facilitated by Tunnelling. Nat. Chem. **2013,** 5, 745-749.

Table 1. Laser induced fluorescence excitation schemes for the detection of OH(v=1-3) and OD(v=1-3).

Species	Probe λ / nm	Transition	Details for Generation of λ
OH(v=1)	346.1	$Q_1(1)\ A^2\Sigma(v=0) \leftarrow X^2\Pi(v=1)$	Excimer / Dye (PTP/DMQ)
OH(v=2)	350.9	$Q_1(1)\ A^2\Sigma(v=1) \leftarrow X^2\Pi(v=2)$	Excimer / Dye (PTP/DMQ)
OH(v=3)	356.7	$Q_1(1)\ A^2\Sigma(v=2) \leftarrow X^2\Pi(v=3)$	Excimer / Dye (PTP/DMQ)
OD(v=1)	334.2	$Q_1(1)\ A^2\Sigma(v=0) \leftarrow X^2\Pi(v=1)$	Nd:YAG / Dye (pyridine) + Doubling
OD(v=2)	338.2	$Q_1(1)\ A^2\Sigma(v=1) \leftarrow X^2\Pi(v=2)$	Nd:YAG / Dye (pyridine) + Doubling
OD(v=3)	342.1	$Q_1(1)\ A^2\Sigma(v=2) \leftarrow X^2\Pi(v=3)$	Nd:YAG / Dye (pyridine) + Doubling

Table 2. Overall bimolecular rate coefficients ($k_{R1total}$) for OH(v=1,2,3) + SO_2 between 295 K and 806 K. The uncertainties are two standard deviations obtained from the linear fits of the bimolecular plots.

Temperature / K	$k_{R1total}$ (v=1) / 10^{-12} cm^3 $molecule^{-1}$ s^{-1}	$k_{R1total}$ (v=2) / 10^{-12} cm^3 $molecule^{-1}$ s^{-1}	$k_{R1total}$ (v=3) / 10^{-12} cm^3 $molecule^{-1}$ s^{-1}
298	1.9 ± 0.3	3.0 ± 0.4	5.1 ± 0.5
434		2.7 ± 0.3	
435			4.9 ± 0.5
436	1.6 ± 0.2		
536	1.6 ± 0.2	2.7 ± 0.3	
541			4.4 ± 0.8
619		2.5 ± 0.3	
621	1.7 ± 0.2		
673		2.5 ± 0.3	
676	1.6 ± 0.2		
755	1.4 ± 0.4		
759		2.2 ± 0.3	
806	1.3 ± 0.5		

Table 3. Overall bimolecular rate coefficients ($k_{R1total}$) for OD(v=1,2,3) + SO_2 between 295 K and 810 K. The uncertainties are two standard deviations obtained from the linear fits of the bimolecular plots.

Temperature / K	$k_{R1total}$ (v=1) / 10^{-12} cm^3 $molecule^{-1}$ s^{-1}	$k_{R1total}$ (v=2) / 10^{-12} cm^3 $molecule^{-1}$ s^{-1}	$k_{R1total}$ (v=3) / 10^{-12} cm^3 $molecule^{-1}$ s^{-1}
298	1.9 ± 0.3	2.7 ± 0.4	4.1 ± 0.6
433			3.8 ± 0.5
435		2.4 ± 0.3	
437	1.6 ± 0.3		
542		2.2 ± 0.3	
543			3.6 ± 0.5
547	1.7 ± 0.3		
616			3.6 ± 0.5
620		2.4 ± 0.3	
625	1.6 ± 0.3		
668		2.4 ± 0.3	
669			4.0 ± 0.6
675	1.7 ± 0.3		
754			4.5 ± 0.8
756		2.7 ± 0.5	
761	1.9 ± 0.4		
810	2.0 ± 0.4		

Table 4. Returned parameters from fitting the OH and OD + SO_2 data to equation 4.

Errors quoted are 1σ.

		OH(v) + SO_2 [a]	OH(v) + SO_2 [b]	OD(v) + SO_2	OH(v) + C_2H_2 [27]
B / 10^{-12} [c]		0.28 ± 0.34	8.2 ± 7.1	35 ± 34	4 ± 6
C / $K^{1/3}$		9.6 ± 9.7	-27.7± 4.7	-36.4 ± 10.4	-14.6 ± 14.2
10^{-4} D / K^2		0 ± 3.7	15 ± 104	15.1 ± 4.0	7.6 ± 3.0
n [d]		2.0 ± 0.26	2.6 ± 0.8	2.0 ± 0.24	2.79 ± 0.43
k_1^∞	A/10^{-12}	0.72 ± 0.33	1.15 ± 0.36	1.04± 0.27	
× $(T/295)^m$	E	0.06 fixed	0.06 fixed	0.06 ± 0.19	
CHISQ/Degrees of Freedom		2.17	7.60	1.17	

[a] In this analysis, boundary condition ensured that D did not go below 0.
[b] In this analysis, boundary condition ensured that D did not go below 1.5×10^5.
[c] Units are cm^3 $molecule^{-1}$ s^{-1}.
[d] Boundary condition ensured that n did not go below 2, the harmonic oscillator limit.

Figure Captions

Figures

Figure 1. Typical OH(v=1) decay in the presence of SO_2 (1.07×10^{16} molecule cm^{-3}) at 295 K, where filled squares are the measured fluorescence intensities. The total pressure is equal to 37.3 Torr and the added H_2 (6.84×10^{16} molecule cm^{-3}) ensures that the $O(^1D)$ is titrated to OH(v). The lines are a biexponential (red) and (from t=50 μs) exponential (blue) fit to the data, where the decay rate coefficients are (2.69 ± 0.39) and (2.29 ± 0.02) $\times 10^4$ s^{-1}, respectively. Note that the red and blue lines converge and this is the point where the culled exponential analysis is carried out (see text for details).

Figure 2. Typical bimolecular plot for OH(v=1) at 295 K, ~ 40 Torr total pressure of He, where the squares and circles are obtained from equations E1 ($k_i[SO_2] = k_{obs}$) and E2, respectively, and linear regression gives bimolecular rate coefficient of (2.24 ± 0.16) and (2.04 ± 0.01) $\times 10^{-12}$ cm^3 $molecule^{-1}$ s^{-1}, respectively.

Figure 3. OH(v=1,2,3) + SO_2 data fitted to composite function that accounts for complex formation and non-reactive VET, SSH-type. The symbols are the data, which includes Blitz et al.,[21] and the red crosses are the best fit (Equation 4, see Table 4 for the fitting parameters). These fitting parameters predict k_1^{∞} = (7.1 ± 3.3) $\times 10^{-13} \times (T/298)^{0.06}$ cm^3 $molecule^{-1}$ s^{-1}, the blue line.

Figure 4. OD(v=1,2,3) + SO_2 data fitted to composite function that accounts for complex formation and non-reactive VET, SSH-type. The symbols are the data and the red crosses are the best fit (Equation 4, see Table 4 for the fitting parameters). These fitting parameters predict $k_1^{\infty} = (10.4 \pm 2.5) \times 10^{-13} \times (T/298)^{0.06}$ cm^3 $molecule^{-1}$ s^{-1}, the blue line.

Figure 5. A qualitative potential energy surface for the reaction between OH + SO_2 based on the findings from this study, where a weakly bound complex, OH-OSO, is initially formed before proceeding to product, HO-SO_2.

TOC Graphic

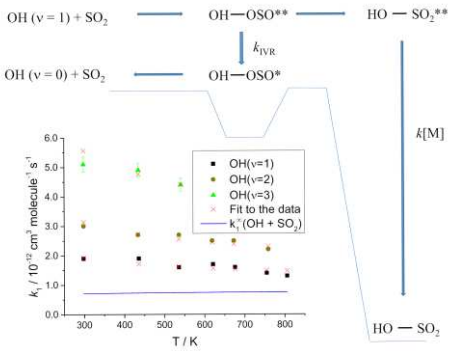
OH (v = 1) + SO2
OH—OSO**
HO — SO2**
kIVR
OH (v = 0) + SO2
OH—OSO*
k[M]
HO — SO2
OH(v=1)
OH(v=2)
OH(v=3)
Fit to the data
k1(OH + SO2)
k1 / 10-12 cm3 molecule-1 s-1
T / K